Heterologous expression of *pharaonis* halorhodopsin in *Xenopus laevis* oocytes and electrophysiological characterization of its light-driven Cl^- pump activity

Akiteru Seki[1], Seiji Miyauchi[1], Saori Hayashi[1], Takashi Kikukawa[2], Megumi Kubo[3], Makoto Demura[3], Vadivel Ganapathy[4] and Naoki Kamo[3]

1 Graduate School of Pharmaceutical Sciences, 2 Laboratory of Biomolecular Systems, Creative Research Initiative "Sosei" (CRIS), 3 Department of Biomolecular Science, Faculty of Advanced Life Sciences, Hokkaido University Sapporo Japan 060-0812 and 4 Department of Biochemistry and Molecular Biology, Medical College of Georgia, Augusta, Georgia 30912

To whom correspondence should be addressed
Seiji Miyauchi, Ph. D. E-mail: miya@pharm.hokudai.ac.jp

Running title: Voltage Dependence of ion pumping by *p*HR

SUMMARY

Natronomonas pharaonis halorhodopsin (*p*HR) is an archaeal rhodopsin functioning as an inward-directed light-driven Cl^- pump. To characterize the electrophysiological features of the Cl^- pump activity of *p*HR, we expressed *p*HR in *Xenopus laevis* oocytes and analyzed its photo-induced Cl^- pump activity using the two-electrode voltage-clamp technique. Photo-induced outward currents were observed only in the presence of Cl^-, Br^-, I^-, NO_3^-, and SCN^- but not in control oocytes, indicating that the photo-induced anion currents were mediated by *p*HR. The relationship between the photo-induced Cl^- current via *p*HR and the light intensity was linear, demonstrating that the transport of Cl^- is driven by a single-photon reaction and that the steady-state current is proportional to the excited *p*HR molecule. The current-voltage (*I-V*) relationship for *p*HR-mediated photo-induced currents was also linear between -150 mV and +50 mV. The slope of the line describing the *I-V* relationship increased as the number of the excited *p*HR molecules was increased by the light intensity. The reversal potential (V_R) for Cl^- as the substrate for the anion pump activity of *p*HR was about -400 mV. The value for V_R was independent of light-intensity, meaning that the reversal potential reflects the intrinsic value of the excited *p*HR molecule. The value of V_R changed significantly for the R123K mutant of *p*HR. We also show that the Cl^- pump activity of *p*HR can generate a substantial negative membrane potential, indicating that *p*HR is the very potent Cl^- pump. We have also analyzed the kinetics of the voltage-dependent Cl^- pump activity as well as that of the photocycle. Based on these data, a kinetic model for the voltage-dependent Cl^- transport via *p*HR is presented.

INTRODUCTION

Halorhodopsin (HR), discovered in the archaebacterium, *Halobacterium*, is an inward-directed Cl^- pump (1-4). HR, functioning as a Cl^- pump, has the ability to transport Cl^- against an electrochemical gradient, and can generate an inside-negative membrane potential to support ATP synthesis (1, 5, 6). Since its original discovery, several HRs from different sources have been reported; but most studies focusing on the functional aspects of HR have used *Halobacterium salinarum* halorhodopsin (sHR) and *Natronomonas pharaonis* halorhodospin (*p*HR) as model systems (4, 7). These two proteins show high similarity in amino acid sequences (identity, 66%; homology, 97%). Based on the high sequence homology between the two Cl^- pumps and their similar photo-induced intermediates, it has been assumed that these proteins have similar structure (8-11).

Recently, the X-ray crystal structure of *s*HR was determined at a resolution of 1.8Å, and it showed striking similarity to that of bacteriorhodopsin (BR) (4, 12, 13). *s*HR is composed of seven α-helices, forming a transmembrane channel-like structure. The channel is divided into a cytoplasmic (CP) and an extracellular (EC) half-channels, separated by the chromophore retinal, which is bound through the Schiff base to Lys242 (12). The crystal structure revealed that Cl^- interacts with the proton of the protonated Schiff base and the hydroxyl group of Ser115 as well the hydrophobic methyl group of Thr111. The crystal structure also indicated that Cl^- is hydrated by a cluster of three water molecules that form hydrogen bonds with neighboring amino acid residues. It is of note that anion binding is observed in the crystal structure only at this position of the EC channel, implying that Cl^- is translocated to the cyotoplasmic space by the photon (12). It is assumed that a Cl^--binding or -interacting site in the cytoplasmic channel is also required for the release of the translocated Cl^- into the cytoplasmic space.

Based on the crystal structure as well as the kinetic analysis of photo-induced intermediates, the vectorial transport of Cl^- via HR is composed of three main processes (6, 9, 11, 12, 14): **(i)** Cl^- binding to the vicinity of the protonated Schiff base region of the retinal chromophore (the EC binding site), **(ii)** Cl^- translocation, and **(iii)** Cl^- release from the CP binding site. The investigation of the electrophysiological features of HR pump activity is very important for a better understanding of the function of the pump at the molecular level. The functional activity of HR has been studied using different experimental approaches (1, 5, 15-19). The function of HR as an inward-directed Cl^- pump has been clarified with cell envelope vesicles from *Halobacterium salinarum* as well as with intact bacteria (1, 5, 20). Spectroscopic and flux measurements under conditions of different membrnae potential have been done with vesicles or bacteria; but these were difficult experiments since precise analysis of voltage dependence is difficult to study with these systems owing to the small size of the bacteria or membrane vesicles. Direct electrical measurements have been undertaken with HR membrane sheets capacitatively coupled to black lipid membranes (15) or to thin films (16-18), and also with membrane suspensions (19). The latter system has an inherent drawback because the orientation of HR cannot be controlled well. Thus, details of the electrophysiological aspects of the Cl^- pump activity of HR are still lacking.

In the present study, we used the *Xenopus laevis* oocyte expression system to elucidate the electrophysiological features of *N. pharaonis* halorhodopsin (*p*HR). In this system, the photo-induced currents due to anion transport could be determined precisely to analyze the kinetics of the transport process. Here we demonstrate that the Cl^- pump activity via *p*HR is dependent on membrane potential. Based on this voltage-dependency, we show for the first time that the value of V_R (reversal potential) at which the pump current by *p*HR becomes zero is an intrinsic

property of the pump independent of light intensity. These studies also show that the Cl^- pump activity by *p*HR can generate a considerable negative membrane potential (about -400 mV), indicating that *p*HR is a highly active Cl^- pump.

MATERIALS AND METHODS

Construction of the expression plasmid of the histidine-tagged pHR in the oocyte expression vector pGH19

The pGH19 vector (kindly provided by Dr. Peter S. Aronson, Yale University School of Medicine) contains the 3'-and 5'-untranslated regions of the *Xenopus* β-globin gene downstream and upstream sides of the cloning site, respectively. The coding region of *p*HR was amplified by PCR using the primers 5'-GATATATAGCCATG ACTGAGACATTGCCACC-3' (sense) and 5'-TAAGCTTCAGTGGTGGTGGTGGTGGTGCTCCAGGTCGTCAGCGGGAGTGC-3' (antisense) and pET21c(+)-*p*HR plasmid (21) as the template. A *Hind*III site (indicated by the *underlining*) was added to the 5'-end of the antisense primer for the purpose of subcloning. The PCR product was first subcloned in a pGEM-T vector (Promega, Madison, MI), and the confirmation of its complete sequence was carried out with the Taq DyeDeoxy terminator method employing an automated PerkinElmer Applied Biosystems 377 Prism DNA sequencer (Foster City, CA). The insert was then released by *Eco*RI/*Hind*III double digestion. The pGH19 vector was linearized with *Eco*RI/*Hind*III and then used for the ligation of the *p*HR cDNA. The resultant product was partially sequenced to confirm the orientation of the insert. The mutant plasmid for the expression of R123K *p*HR was constructed with a Quickchange site-directed mutagenesis (Stratagene Cloning Systems, San Diego, CA) as described previously (14). The mutation introduced into the plasmid was also confirmed by sequencing.

Functional expression of the histidine-tagged pHR in Xenopus laevis oocytes

The amplified *p*HR cDNA was expressed heterologously in *Xenopus* oocytes by cRNA injection. Capped cRNA was synthesized using mMESSAGE mMACHINE kit (Ambion Inc., Austin, TX). Mature oocytes (stage V-VI) from *Xenopus* were isolated by treatment with collagenase (1.6 mg/ml), manually defolliculated, and maintained at 18 ^{o}C in modified Barth's medium, supplemented with 3 μM retinal and 50 μg/ml gentamicin as described previously (22, 23). On the following day, oocytes were injected with 50 ng *p*HR cRNA in a 50 nl volume and incubated for 3 – 5 days. The oocytes were used for electrophysiological studies 3 - 5 days after cRNA injection. Electrophysiological studies were performed with two-electrode voltage-clamp (TEVC) technique as described previously. The oocyte was superfused with perfusion buffer (96 mM NaCl, 2 mM KCl, 1 mM $MgCl_2$, 1 mM $CaCl_2$, 10 mM Hepes and 6 mM Tris, pH7.5). After the current stabilized, the oocyte was superfused with the uptake buffer. The oocyte was voltage-clamped at -50 mV. The composition of the uptake buffer was 2 mM Kgluconate , 1 mM $Mg(gluconate)_2$, 1 mM $Ca(gluconate)_2$, 10 mM Hepes and 100 mM sodium salt (NaCl , NaBr, NaI, NaSCN, $NaNO_3$ or sodium 2-(N-morpholino)ethanesulfonate (NaMes)), pH 7.5. The current-voltage (*I-V*) relationship was analyzed immediately before and within a few seconds after illumination with green light (530 ± 18 nm) when the current reached the maximum and steady state. The green light was produced by a light-emitting diode, Luxeon V Star (Lumileds Lighting Co., San Jose, CA). The measurements of currents at different membrane potential were made using short pulses (100 ms) in the range of –150 mV to +50 mV in 20-mV increments. Each pulse was separated with a pause (250 ms). TVEC experiments were performed with TVEC amplifier, CEZ-1250 (Nihon Kohden Industry Ltd., Tokyo, Japan) and a commercially available program (Clampex software, Axon Instruments). The photo-induced current at each applied voltage was calculated as the difference between the steady state currents recorded before and after illumination. Saturation kinetics of photo-induced currents associated with the anion pump activity was analyzed with seven different concentrations of NaX ($X = Cl^-$, Br^-, NO_3^-, SCN^-

and I$^-$). The light-induced currents are defined by the kinetic parameters I_{max} (the maximal photo-induced current) and $K_{0.5}$ (the anion concentration necessary for the induction of half-maximal current). The data for the photo-induced current (I) were fitted to the following Michaelis-Menten equation, describing a single saturable component, by an iterative nonlinear least-squares method (Origin, MicroCal, Northampton, MA):

$$I = \frac{I_{max}[s]}{K_{0.5} + [s]} \qquad \text{Eq.1}$$

where [s] is the concentration of the transportable anion in the perfusion buffer.

Protein expression and purification of the histidine-tagged pHR

The experimental details for protein expression and purification employing *E. coli* BL21- (DE3) cells have been described in a previous paper (21). Fractions of the proteins using Ni-NTA agarose (Qiagen, Hilden, Germany) were collected by elution (flow rate, 56 mL/h) with buffer E (50 mM Tris- HCl (pH 7.0), 300 mM NaCl, 150 mM imidazole, and 0.1% *n*-dodecyl α-D-maltopyranoside [dodecyl maltoside (DM)] (Dojindo Lab, Kumamoto, Japan)). The yield of the recombinant *p*HR was almost the same as reported previously (21).

Flash photolysis spectroscopy

The photocycle of *p*HR was analyzed by flash spectroscopy with a computer-controlled flash-photolysis apparatus for measuring transient absorption changes every 0.5 μs in the time range from 10 μs to 220 ms. The computer-controlled flash-photolysis apparatus was constructed as described previously (14). The absorbance of the sample in 50 - 1000 mM NaCl [containing 10 mM MOPS (pH 7.0) and 0.1% DM] was 0.5 at the absorption maximum, and the temperature was maintained at 20 ^{o}C.

Data analysis of photocycling

The data collected at all wavelengths from 410 to 710 nm were fitted to a multiexponential equation. SVD analysis of the observed data confirmed the existence of 4 kinetically distinguishable photo-induced intermediates (14). The spectrum of the *i*th-intermediate, P_i and its decay time constant, τ_i were calculated according to the Chizhov and Engelhard (11, 14).

RESULTS

Induction of photo-induced outward currents by Cl^- and other anions in pHR-expressing Xenopus oocytes

The photo-induced currents were monitored under voltage-clamp conditions in oocytes after 3-5 days following microinjection of *p*HR cRNA. When *p*HR-expressing oocytes were illuminated with green light (λ_{max} = 530 ± 18 nm) from the light-emitting diode, the presence of Cl^- in the perfusion buffer induced marked outward currents (Fig.1). Similar currents were also observed with other anions such as Br^- and I^-, NO_3^- or SCN^-. These currents were however specific since the substitution of Cl^- with Mes^- failed to induce detectable currents. Uninjected oocytes and oocytes injected with water did not show photo-induced currents in the presence of Cl^- with or without incubation of the oocytes with retinal (data not shown). These data demonstrate that *p*HR is able to transport Cl^-, Br^-, I^-, NO_3^-, and SCN^-, and that the transport process is associated with the induction of outward currents. Outward currents in oocytes under voltage-clamp conditions indicate the transfer of negative charges into the oocytes, suggesting that *p*HR-mediated entry of Cl^- and other anions into the oocytes is responsible for the outward currents. It is known that *p*HR transports not only Cl^- and other halides (Br^- and I^-) but also NO_3^- and SCN^- (5, 24-26). Our electrophysiological data with *p*HR, expressed heterologously in *Xenopus* oocytes, confirm these earlier observations.

Voltage-dependence and reversal potential (V_R) for pHR-mediated anion pump activity

We then characterized the anion pump activity of *p*HR by using the photo-induced anion-dependent outward currents as the read-out of the activity. Figure 2 summarizes the current-voltage (*I-V*) relationship and anion-dependent photo-induced currents at -50 mV. The *I-V* curve showed linearity in the measurable range of membrane potential (from -150 mV to +50 mV) (Fig.2A). At -50 mV, the order of the anion-dependent current induced by photons is: $Cl^- = Br^- > I^- > NO_3^- > SCN^-$ (Fig.2B). The *I-V* relationship data were extrapolated to determine the x-intercepts (*i.e.*, zero current), which correspond to the reversal potentials (V_R) for different anions. The values for V_R for different anions ranged from -250 mV to -450 mV (Fig.2C): The V_R for Br^- is the most negative, followed by that for Cl^- and I^-.

The voltage dependency of the photo-induced current via *p*HR-mediated Cl^- transport was determined at different light intensities (Fig.3). The magnitude of the photo-induced and Cl^--dependent currents via *p*HR was linear with light intensity initially but began to plateau subsequently (Fig.3A). The profile of the curve indicated that the transport of Cl^- is driven by a single-photon reaction and that the steady-state current is proportional to the excited *p*HR molecule. The slope of the lines describing *I-V* relationship increased as the light intensity increased (Fig3B). The x-intercept values were similar (~-400 mV) at all light intensities tested, showing that the reversal potential (V_R) is independent of light intensity and that this value represents an intrinsic characteristic of the excited *p*HR molecule. This is further substantiated by the significant change in V_R for the Arg123 (R123K) mutant (Fig.4). Arg123 is critical for Cl^- recognition and transport, and when this amino acid is mutated, it changes the Cl^- pump activity and the reversal potential. Taken collectively, the data show that the Cl^- pump activity of *p*HR is robust and that the pump can theoretically generate a large negative membrane potential (~-400 mV) in the presence of extracellular Cl^-.

Kinetics of photo-induced currents associated with pHR-mediated Cl^- pump activity

Employing Cl^- as the substrate, we analyzed the saturation kinetics of photo-induced currents in *p*HR-expressing oocytes. The relationship between the photo-induced current and Cl^- concentration at different membrane potentials is described in Fig.5. The photo-induced outward

currents were saturable with increasing concentrations of Cl^- at all membrane potentials examined. The inset in Fig. 5 shows the Eadie-Hofstee plot at a membrane potential of -50 mV. The kinetic parameters were calculated by fitting data to Eq. 1; estimated values were: $K_{0.5}$ (concentration of Cl^- needed for the half-maximal photo-induced current) = 24.0 $\pm$ 2.5 mM (mean $\pm$ SE) and I_{max} (maximal photo-induced current) = 324 $\pm$ 22 nA (mean $\pm$ SE). Under the conditions employed in the present studies, the dissociation constant of *p*HR for Cl^- is thus estimated to be about 25 mM. Similar experiments were conducted with other anions recognized by *p*HR and kinetic parameters were calculated for each of them (Table I). The order of the reciprocal of $K_{0.5}$ value reflecting a binding affinity of anion is: Br^-> I^->Cl^->SCN^-> NO_3^-. The $K_{0.5}$ value seems to be related to the size of the hydrated anions. The order of I_{max} value is: Cl^- >Br^->I^->NO_3^->SCN^-.

The dependency of the kinetic parameters, $K_{0.5}$ and I_{max}, on membrane potential is described in Fig. 6. The I_{max} decreased as the membrane potential became more negative, indicating that the rate determining process in *p*HR-mediated Cl^- transport is dependent on membrane potential. The $K_{0.5}$ also showed marked changes when membrane potential was altered. The value increased markedly as the membrane potential became more negative, implying that the apparent affinity for Cl^- decreased at more negative membrane potentials.

The photocycle of pHR with varying Cl^- concentrations

To evaluate the Cl^--dependent and the rate determining processes during the photocycle reaction, we analyzed the photocycle of *p*HR at different concentrations of Cl^- (0.05 - 1 M). The absorbance values observed at different wavelengths (410 - 710 nm) were fitted simultaneously with four exponentials, since SVD analysis and the calculation of standard deviation concluded the existence of 4 intermediates. The spectra of the kinetically distinguishable photo-induced intermediates were given in Fig.7A. The spectra of P_1 and P_2 were almost the same, and the absorption maximum (λ_{max}) was approx. 520 nm, whereas the spectrum of P_4 showed the same absorption maximum as the original pigment. The profiles of P_1, P_2 and P_4 intermediates were independent of Cl^- concentration. The decay time constants (τ_1 and τ_2) were also independent of Cl^- concentration (Fig.7B). The P_1 and P_2 intermediates are identified as L_1 and L_2 intermediates, respectively, as indicated by the spectral profile and the decay time constants. Judging from the spectra and the extremely long time constant, the P_4 intermediate is identified as *p*HR' intermediate. On the other hand, the spectra of P_3 intermediate had two absorption maxima, implying that P_3 is comprised of at least two physically defined intermediates that attain equilibrium promptly. Only the P_3 spectrum revealed large Cl^- dependency where considerable shift of the equilibrium occurs from one intermediate with λ_{max} at ~ 610 nm to the other with λ_{max} at ~510 nm. The intermediate with λ_{max} at ~ 610 nm can be thought to be Cl^--free, because the λ_{max} value is attributed to a Cl^--free environment of the protonated Schiff base (21, 24, 26). Váró *et al* (9, 10) and Chizhov and Engelhard (11) also described the fast equilibrium between anion-bound and anion-free states in the photocycle. The shift of the equilibrium in the P_3 intermediate with changes in Cl^- concentration means that this intermediate is involved in the interaction between Cl^- and *p*HR. The decay time constant (τ_3) decreased markedly as Cl^- concentration increased. Judging from the photocycle sequence and the acceleration of the transition rate from P_3 to P_4 (*p*HR') by the external Cl^-, we conclude that the transition is involved in the Cl^- binding process. Váró *et al* (9, 10) also demonstrated that the process of Cl^- binding to *p*HR becomes faster as the external Cl^- concentration is increased.

DISCUSSION

In this paper, we report on the successful expression of functional *p*HR in *Xenopus laevis* oocytes for electrophysiological characterization of its anion pump activity. This has allowed us to carry out a detailed analysis of the photo-induced anion-dependent outward currents associated with *p*HR-mediated entry of anions into the oocyte. As can be seen in Fig.1, photo-induced outward currents were detectable only in *p*HR-expressing oocytes when the oocytes were superfused with anions such as Cl^-. Substrate specificity studies showed that *p*HR can recognize and pump a variety of anions, including not only monoatomic (*e.g.*, Cl^-, Br^-, I^-) but also polyatomic (*e.g.*, NO_3^-, SCN^-) anions. These data are in accordance with those reported previously (5, 24, 26). The photo-induced currents showed saturation kinetics with all anions that were transported via *p*HR. Duschl and Lanyi have also determined the Cl^- transport activity via *p*HR employing envelope vesicles from *N. pharaonis* (5). The concentration dependency of Cl^- transport activity by *p*HR followed the Michaelis-Menten type kinetics with a single saturable component. The $K_{0.5}$ value for Cl^- reported by Duschl and Lanyi was 25 mM, consistent with the present data. The $K_{0.5}$ value, which approximates the dissociation constant for the interaction of the transporter with its substrate, was determined for five different anions (Table I). Based on these data, the rank order of substrate affinity is as follows: Br^-> I^->Cl^->SCN^-> NO_3^-. The order of the affinity seems dependent on the size of hydrated rather than dehydrated anions, because there is good correlation between the $K_{0.5}$ value and the reciprocal of the limiting equivalent conductivity (λ^0) of anions in water (Fig.8A). In general, the λ^0 value reflects the mobility of ion in water which is dependent on the Stokes radius of ion. Using the spectroscopic analysis of the binding of different anions to *s*HR, Schobert and Lanyi demonstrated that the binding affinity is related not to the dehydrated radius of the transportable anion, but to the Stockes (*i.e.*, hydrodynamic) radius, which reflects the radius of the hydration shell around the anion (27). On the basis of the crystal structure of *s*HR, the binding pocket of Cl^- is composed of the protonated Schiff base, Ser115, Arg108, Asp215 and Trp112. It is noted that the anion Cl^- remained still partially hydrated by a cluster of three water molecules (12), suggesting that the binding pocket has enough room to accommodate anions with different sizes. This is one of the reasons why the affinity of anions is dictated by the radius of the hydration shell around the anion. In contrast to the $K_{0.5}$ values, the capacity of the pump activity, I_{max}, is dependent on the dehydrated sizes of the anions (Fig. 8B); the rank order of the maximal capacity of the pump activity is as follows: Cl^->Br^- >I^->NO_3^->SCN^- (Fig.8B). These results suggest that the rate determining step in the transport cycle shows a dependency on the size of dehydrated ion. Recently, using FTIR spectroscopic analysis data, Shibata *et al.* have demonstrated that the hydrophobicity of the environment in the vicinity of the protonated Schiff base is involved in the translocation of the anion from EC binding site to CP binding site (28). The anion might be dehydrated when it is translocated from EC binding site to CP binding site (12).

It is interesting to note that the anion pump activity of *p*HR shows voltage dependence. The *I-V* relationship is linear over the range of membrane potential employed (between -150 and +50 mV). The profile of the *I-V* relationship remains unchanged irrespective of the illumination intensity (Figs.2 and 3). The slope of *I-V* curve increased as the number of the excited *p*HR molecule increased by the light intensity, whereas the reversal potential, obtained by the extrapolations of the lines describing the *I-V* relationship, did not change with different intensities of light. It seems plausible that the slope of the line describing the *I-V* relationship is a factor of the number of the photo-excited *p*HR molecules. The linear relationship between photo-induced current and the illumination intensity (Fig.3) demonstrates that the transport of Cl^-

via *p*HR is driven by a single photon. On the other hand, the value of V_R changed markedly for the mutant of Arg123 (R123K) (Fig.4). Since Arg123 is very critical for the binding and transport of the substrates, the change in V_R as a consequence of mutation of this particular residue suggests that V_R directly reflects the intrinsic ion motive force of the *p*HR pump. On the basis of this voltage-dependency, we show for the first time that the V_R value at which the pump current is reduced to zero reflects the intrinsic motive force of the excited *p*HR molecule to pump Cl^- into cell. On the basis of the thermodynamic theory, the Gibbs free energy for the transport of Cl^- by the excited *p*HR molecule (ΔG_{imf}) is given by the following equation, since one chloride anion is transported per one photon absorption;

$$\Delta G_{imf} = z_i F V_R \qquad \text{Eq.2}$$

where z_i and F represent the valence of the anion and the Faraday's constant, respectively. According to Eq.2, the ΔG_{imf} value was estimated with V_R value -400 mV to be -38.6 (kJ/mol). Employing the Plank's constant, the quantum energy for one mole of photon at 580 nm (ΔE_{photon}) is calculated to be 206 (kJ/mol). The probability that *p*HR absorbs the light quantum energy, followed by the excitation of *p*HR, *i.e.*, the isomerization of the retinal from all-*trans* to 13-*cis*, is assumed to be 50 %. On the basis of a single photon reaction, the conversion efficiency from the energy of the photon stored in the retinal isomerization to the Cl^- translocation energy is 18.7 %.

It has been well characterized that the light-driven pump BR from *H. salinarum* can generate the electrochemical potential of up to -280 mV inside the cell (29), which corresponds to a proton motive force to be used for ATP synthesis and is coupled to other secondary active transporters in the plasma membrane. Nagel *et al.* also estimated the V_R value on the basis of the extrapolation of the line describing the *I-V* relationship in *Xenopus* oocyte expressing BR to be -220 mV, which is in accordance with the electrochemical potential for proton (30). It should be noted that the Cl^- pumping activity by *p*HR can generate a more negative membrane potential, -400 mV, compared with that of BR. The substantial negative V_R of *p*HR implies that it is a much more effective anion pump than BR.

As shown in Figs 2 and 3, the uniqueness of *I-V* relationship resides in the linear nature of the relationship. This raises an interesting question: What is the mechanism for the voltage-dependent change in the anion pump activity of this transporter? In other words, which particular step(s) in the anion pumping via *p*HR is (are) regulated by the electric field? The photo-induced current was saturable with respect to Cl^- concentration and followed Michaelis-Menten type kinetics (Fig.5). Both $K_{0.5}$ and I_{max} values showed voltage-dependency; the $K_{0.5}$ value increased when the membrane potential became more negative, whereas the I_{max} value decreased. It is of note that the *I-V* relationship is mainly governed by the voltage-dependent $K_{0.5}$ and I_{max} values. In order to clarify which step in the photocycle is related to these kinetic parameters with regard to Cl^- pumping, we performed flash-photolysis analysis with different Cl^- concentrations (Fig.7). In this analysis, we evaluated the rate determining process as well as the Cl^--dependent processes, because of two reasons: (i) all intermediates attain steady state under conditions of continuous illumination and the excited *p*HR consists almost entirely of the population of the intermediate molecules in the rate determining transition and (ii) the photo-induced currents at steady state show Cl^- dependency. It is feasible that a kinetic model describing the photo-induced current at steady state can be simplified as shown in Fig.9. On the basis of these properties of photochemical reaction, we have developed the kinetic model describing the photo-induced current at steady state (See Appendix and Fig.9). The scheme is comprised of two processes: one

is the fast transition of intermediates corresponding to Cl^- translocating and releasing processes, and the other is the rate determining transition corresponding to Cl^- binding processes. The photo-induced current is reduced to the following simple equation:

$$I = \frac{k_{rate} P^* F [Cl^-]}{\frac{k_a}{k_d} + [Cl^-]} \qquad \text{Eq.3}$$

where k_a and k_d represent the association and dissociation rate constants for Cl^- binding to EC site, respectively, k_{rate} is the rate constant for the rate determining transition, i.e., *p*HR'→*p*HR transition, P^* is the *p*HR molecule involved in the photo-induced current, and F is the Faraday's constant. Analysis of the data with Eq.3 shows that the voltage-dependence of I_{max} is attributed to the *p*HR'→*p*HR transition which decreased as the membrane potential became more negative. The $K_{0.5}$ value increased as the membrane potential became more negative, implying that the transition is decreased, *i.e.*, the association rate is decreased and/or the dissociation rate is increased as the membrane potential became more negative. Taking the negative charge of Cl^- into account, we hypothesize that, during the vectorial transport of Cl^-, there exists an electrical field in the EC channel affecting Cl^- uptake from the EC bulk space.

The binding of various anions has been studied extensively using detergent-solubilized *p*HR (21, 24, 26). On the basis of absorption wavelength shift caused by the binding of anion to *p*HR, it has been concluded that the Cl^- binding site has a binding constant of 1-2 mM. Other halides also bind strongly to *p*HR. On the other hand, the $K_{0.5}$ values reflecting the binding constants of anions in our studies (Table I) are at least one-order of magnitude larger than the binding constants of anions for detergent-solubilized *p*HR. There are multiple factors that might explain the difference. The kinetic constants for anion binding to detergent-solubilized *p*HR were determined from the absorption wavelength shift caused by the binding of the anion to the transporter protein (21, 24, 26). In contrast, we determined the kinetic constants from the photo-induced outward currents associated with the transport of anions via *p*HR. The binding of the substrate represents only one of multiple steps involved in the transport process. What we determined in our studies is the kinetic constant for the entire transport process rather than for just the binding of the substrate. In addition, membrane potential might have contributed to the differences between the studies. In our oocyte expression system, measurements of *p*HR function were made in the presence of membrane potential which induces electrical field in the EC channel of the transporter. According to stopped-flow experiments on the anion binding to detergent-solubilized *p*HR, Cl^- transport via the transporter occurs mostly by passive diffusion through the EC channel (21). This process is likely to be affected markedly by the alterations in the EC channel induced by the electrical field. Furthermore, the binding process of Cl^- is coupled to an electrogenic event in the cycle. If the binding site is not available when the occupancy of an intermediate state at this event is lowered by the external potential, the apparent affinity of the binding will be lowered depending on the membrane potential. It is recognized however that the membrane potential provides only a partial explanation to the discrepancy in the kinetic constant values. This is because the value for $K_{0.5}$ is ~15 mM when the membrane potential is zero (Fig. 6), and this value is still many times higher than the value obtained with detergent-solubilized *p*HR. The discrepancy between two experimental systems may also be related to the possibility that Cl^- binds to different states of *p*HR depending on the experimental system. The binding constant to *p*HR expressed in *Xenopus* oocytes corresponds to the binding to the intermediate (Fig.9) whereas the binding constant to detergent-solubilized *p*HR corresponds to binding to the ground state.

On the basis of the crystal structure of *s*HR, the Cl^- binding site is located in the vicinity of the protonated Schiff base, 18 Å below the extracellular membrane surface, *i.e.*, Cl^- is stuck on one-third of its pathway through the membrane (12, 13). Supposing that the membrane potential is evenly imposed through the perpendicular vector to the membrane, the membrane potential from the EC bulk space to EC binding site is one-third of the whole membrane potential. As shown in Fig.6, the $K_{0.5}$ value increased almost linearly when the membrane potential was made gradually more negative. Supposing that the increase in $K_{0.5}$ values is governed by the Nernst equation, the imposed membrane potential through the EC channel can be estimated to be 20 % of the whole membrane potential. If the membrane potential is -200 mV, the membrane potential of -40 mV might be imposed at least through the EC channel, which corresponds to 60 % of the voltage difference in the EC channel theoretically calculated on the basis of the linear membrane potential gradient. In contrast to the formation of the membrane potential gradient through the EC channel in *p*HR, the hydrogen bond network is formed through the EC channel in BR, which facilitates proton moving through the EC channel. This hydrogen-network is believed to be a proton-wire that can rapidly transfer the proton through the EC channel in BR (31, 32). Thus, there is no electrical field through the EC channel in BR.

Under conditions of continuous illumination, the photo-induced current attains a steady state. The photo-induced current is governed by the rate determining step, which is also regulated by the applied electrical field. According to Michaelis-Menten kinetics, the I_{max} value reflects the rate determining step. On the basis of the flash photolysis analysis, the I_{max} value is a function of the transition rate constant k_{rate} and the photo-excited molecule of *p*HR. The I_{max} value reflects the transition of *p*HR'→*p*HR, which was estimated to be 10-fold smaller than any other transition in the photocycle. It is important to note that the transition of *p*HR'→*p*HR is also regulated by the applied electrical field. On the basis of the binding analysis of Cl^- to *p*HR with stopped-flow experiments (21), the time course of the binding to *p*HR was composed of two phases, indicating that the uptake process of Cl^- through the EC channel is associated with a subtle conformational change or the subtle distortion of the retinal accompanying an intramolecular charge movement. Previously, Manor *et al.* determined the effect of membrane potential on photochemical reactions of three archaerhodospins in *H. salinarum*, sensory rhodopsin I, BR and *s*HR (20). Each of the three exhibits a decreased rate of thermal decay of the principal photo-induced intermediate when de-energized cells are energized artificially to generate a more negative membrane potential. The intramolecular charge movements with a vectorial component normal to the plane of the membrane possibly occur in the rate-determining thermal steps of each of the three pigments. In other words, a voltage-dependent conformational change common to their respective photocycles might occur. Especially, with regard to BR and HR functioning as ion pumps, these conformational movements might be involved in the electrogenic transport associated with the photocycles. Further analysis of this voltage-dependence of the rate determining step might provide a better insight into the mechanism of the subtle conformational change. The exact mechanism remains yet to be elucidated.

In summary, we have established a *N. pharaonis* halorhodopsin (*p*HR) expression system in *Xenopus laevis* oocytes to gain a better insight into the mechanism of the electrogenic anion transport via *p*HR. In this system, the photo-induced currents due to anion transport could be determined precisely to analyze the kinetics of the transport process. With this approach, we were able to demonstrate that the Cl^- pump activity via *p*HR is dependent on membrane potential. On the basis of this voltage-dependency, we show for the first time that the V_R value, at which the pump current by *p*HR is reduced to zero, represents the intrinsic ion motive force of the

excited *p*HR molecule to pump Cl^- into cell. The Cl^- pumping activity by *p*HR can generate a substantial negative membrane potential, -400 mV, *i.e.*, *p*HR functions as a very potent anion pump.

APPENDIX

It has been demonstrated clearly that Cl^- transport into cells via HR is coupled to the cyclic photochemical reaction of HR molecule: all *trans* to 13-*cis* isomerization of the retinal induced by absorption of a light quantum initiates the photochemical reaction, followed by the thermal reisomerization to the initial all *trans* state. Under conditions of continuous illumination, all intermediates attain steady state and the excited *p*HR consists almost entirely of the population of the intermediate molecules in the rate determining transition. The photo-induced current is governed mainly by the rate determining process. The photo-induced current is also dependent on the external Cl^- concentration (Fig.4). Therefore, focusing only on the intermediates involved in the photo-induced current at steady state, we simplify the photocycle scheme of *p*HR and construct a kinetic model describing the photo-induced current due to Cl^- transport via *p*HR (Fig. 9). The kinetic model is comprised of two processes: one is the fast transition of intermediates corresponding to Cl^- translocating and releasing processes, and the other is the rate determining transition corresponding to Cl^- binding processes. According to the mass conservation, a mass-balance equation consists of the original *p*HR, the photo-excited *p*HR (*p*HR*) molecules, and the Cl^- free and bound intermediates (X_{free} and X_{bound}, respectively).

$$\frac{d(A_{pHR} + A_{pHR^*})}{dt} = k_{rate} A_{X_{bound}} - k_{fast} A_{pHR^*} \qquad \text{Eq.A1}$$

$$\frac{dA_{X_{free}}}{dt} = k_{fast} A_{pHR^*} + k_d A_{X_{bound}} - k_a [Cl] A_{X_{free}} \qquad \text{Eq.A2}$$

$$\frac{dA_{X_{bound}}}{dt} = k_a [Cl] A_{X_{free}} - (k_d + k_{rate}) A_{X_{bound}} \qquad \text{Eq.A3}$$

where A_{pHR}, A_{pHR^*}, $A_{X_{free}}$ and $A_{X_{bound}}$ represent the amounts of original *p*HR, *p*HR*, X_{free} and X_{bound} intermediates, respectively; k_{fast} and k_{rate} are the rate constants with regard to the fast transition and rate-determining transition processes, respectively; k_a and k_d are the association and dissociation rate constants with regard to Cl^- binding to the EC site in *p*HR. Alternatively, the following equation with regard to the total amount of excited *p*HR molecules involved in the photo-induced current cycle holds as follows;

$$P^* = A_{pHR^*} + A_{X_{free}} + A_{X_{bound}} \qquad \text{Eq.A4}$$

where P^* is the total amount of *p*HR molecules involved in the photo-induced current cycle. Under conditions of continuous illumination, all intermediates attain steady state and all mass-balance equations described above are equal to zero. Combining all equations, solving of the term, and substituting the value into Eq.A4 yields the following equation:

$$P^* = k_{rate} A_{X_{bound}} \left(\frac{1}{k_{fast}} + \frac{\frac{k_d + k_{rate}}{k_a}}{k_{rate}[Cl]} + \frac{1}{k_{rate}} \right) \qquad \text{Eq.A5}$$

All intermediates attain steady state and all transition rates are equal. Thus, the photo-induced current at steady-state is expressed as the multiplicity of $A_{X_{bound}}$ with k_{rate} and Faraday's constant, *F* as follows:

$$I = k_{\mathrm{rate}} F A_{X_{bound}} = \frac{P^{*} F}{\frac{k_{\mathrm{d}} + k_{\mathrm{rate}}}{k_{\mathrm{a}}}} \frac{1}{k_{\mathrm{fast}}} + \frac{1}{k_{\mathrm{rate}}}$$ Eq.A6

Taking into consideration that the k_{rate} value is much smaller than any other rate constants (k_{fast}, k_{a} and k_{d}), Eq.A6 is reduced to:

$$I = k_{\mathrm{rate}} F A_{X_{bound}} = \frac{k_{\mathrm{rate}} P^{*} F [Cl]}{\frac{k_{\mathrm{d}}}{k_{\mathrm{a}}} + [Cl]}$$ Eq.A7

Substitutions of $k_{\mathrm{rate}} P^{*} F$ with $I_{\max}$ and the ratio $\frac{k_{\mathrm{d}}}{k_{\mathrm{a}}}$ with $K_{0.5}$ yield the Michaelis-Menten type equation (Eq.1),

$$I = k_{\mathrm{rate}} F A_{X_{bound}} = \frac{I_{\max} [Cl]}{K_{0.5} + [Cl]}$$ Eq.A8

The ratio of P^{*} to the unexcited original *p*HR is designated as α. P* is expressed as the following equation:

$$P^{*} = \frac{\alpha}{\alpha + 1} P_{\mathrm{total}}$$ Eq.A9

where P_{total} is the total amount of the *p*HR protein expressed in the plasma membrane of *Xonopus* oocyte. Substitution of Eq9A into Eq.7A explains why the photo-induced current is proportional to the intensity of illumination in the range of low intensity as shown in Figure 3.

References

1. Schobert, B. and J. K. Lanyi 1982. Halorhodopsin is a light-driven chloride pump. J Biol Chem, *257:* 10306-10313.
2. Mukohata, Y. and Y. Kaji 1981. Light-induced membrane-potential increase, ATP synthesis, and proton uptake in Halobacterium halobium, R1mR catalyzed by halorhodopsin: Effects of N,N'-dicyclohexylcarbodiimide, triphenyltin chloride, and 3,5-di-tert-butyl-4-hydroxybenzylidenemalononitrile (SF6847). Arch Biochem Biophys, *206:* 72-76.
3. Lanyi, J. K. 1990. Halorhodopsin, a light-driven electrogenic chloride-transport system. Physiol Rev, *70:* 319-330.
4. Varo, G. 2000. Analogies between halorhodopsin and bacteriorhodopsin. Biochim Biophys Acta, *1460:* 220-229.
5. Duschl, A., J. K. Lanyi, and L. Zimanyi 1990. Properties and photochemistry of a halorhodopsin from the haloalkalophile, Natronobacterium pharaonis. J Biol Chem, *265:* 1261-1267.
6. Rudiger, M. and D. Oesterhelt 1997. Specific arginine and threonine residues control anion binding and transport in the light-driven chloride pump halorhodopsin. Embo J, *16:* 3813-3821.
7. Lanyi, J. K., A. Duschl, G. W. Hatfield, K. May, and D. Oesterhelt 1990. The primary structure of a halorhodopsin from Natronobacterium pharaonis. Structural, functional and evolutionary implications for bacterial rhodopsins and halorhodopsins. J Biol Chem, *265:* 1253-1260.
8. Varo, G., L. Zimanyi, X. Fan, L. Sun, R. Needleman, and J. K. Lanyi 1995. Photocycle of halorhodopsin from Halobacterium salinarium. Biophys J, *68:* 2062-2072.
9. Varo, G., L. S. Brown, J. Sasaki, H. Kandori, A. Maeda, R. Needleman, and J. K. Lanyi 1995. Light-driven chloride ion transport by halorhodopsin from Natronobacterium pharaonis. 1. The photochemical cycle. Biochemistry, *34:* 14490-14499.
10. Varo, G., R. Needleman, and J. K. Lanyi 1995. Light-driven chloride ion transport by halorhodopsin from Natronobacterium pharaonis. 2. Chloride release and uptake, protein conformation change, and thermodynamics. Biochemistry, *34:* 14500-14507.
11. Chizhov, I. and M. Engelhard 2001. Temperature and halide dependence of the photocycle of halorhodopsin from Natronobacterium pharaonis. Biophys J, *81:* 1600-1612.
12. Kolbe, M., H. Besir, L. O. Essen, and D. Oesterhelt 2000. Structure of the light-driven chloride pump halorhodopsin at 1.8 A resolution. Science, *288:* 1390-1396.
13. Essen, L. O. 2002. Halorhodopsin: light-driven ion pumping made simple? Curr Opin Struct Biol, *12:* 516-522.
14. Sato, M., M. Kubo, T. Aizawa, N. Kamo, T. Kikukawa, K. Nitta, and M. Demura 2005. Role of putative anion-binding sites in cytoplasmic and extracellular channels of Natronomonas pharaonis halorhodopsin. Biochemistry, *44:* 4775-4784.
15. Bamberg, E., P. Hegemann, and D. Oesterhelt 1984. Reconstitution of halorhodopsin in black lipid membranes. Prog Clin Biol Res, *164:* 73-79.
16. Kalaidzidis, I. V., Y. L. Kalaidzidis, and A. D. Kaulen 1998. Flash-induced voltage changes in halorhodopsin from Natronobacterium pharaonis. FEBS Lett, *427:* 59-63.

17. Okuno, D., M. Asaumi, and E. Muneyuki 1999. Chloride concentration dependency of the electrogenic activity of halorhodopsin. Biochemistry, *38:* 5422-5429.
18. Muneyuki, E., C. Shibazaki, H. Ohtani, D. Okuno, M. Asaumi, and T. Mogi 1999. Time-resolved measurements of photovoltage generation by bacteriorhodopsin and halorhodopsin adsorbed on a thin polymer film. J Biochem (Tokyo), *125:* 270-276.
19. Ludmann, K., G. Ibron, J. K. Lanyi, and G. Varo 2000. Charge motions during the photocycle of pharaonis halorhodopsin. Biophys J, *78:* 959-966.
20. Manor, D., C. A. Hasselbacher, and J. L. Spudich 1988. Membrane potential modulates photocycling rates of bacterial rhodopsins. Biochemistry, *27:* 5843-5848.
21. Sato, M., T. Kanamori, N. Kamo, M. Demura, and K. Nitta 2002. Stopped-flow analysis on anion binding to blue-form halorhodopsin from Natronobacterium pharaonis: comparison with the anion-uptake process during the photocycle. Biochemistry, *41:* 2452-2458.
22. Miyauchi, S., E. Gopal, Y. J. Fei, and V. Ganapathy 2004. Functional identification of SLC5A8, a tumor suppressor down-regulated in colon cancer, as a Na(+)-coupled transporter for short-chain fatty acids. J Biol Chem, *279:* 13293-13296.
23. Gopal, E., Y. J. Fei, M. Sugawara, S. Miyauchi, L. Zhuang, P. Martin, S. B. Smith, P. D. Prasad, and V. Ganapathy 2004. Expression of slc5a8 in kidney and its role in Na(+)-coupled transport of lactate. J Biol Chem, *279:* 44522-44532.
24. Scharf, B. and M. Engelhard 1994. Blue halorhodopsin from Natronobacterium pharaonis: wavelength regulation by anions. Biochemistry, *33:* 6387-6393.
25. Balint, Z., M. Lakatos, C. Ganea, J. K. Lanyi, and G. Varo 2004. The nitrate transporting photochemical reaction cycle of the pharaonis halorhodopsin. Biophys J, *86:* 1655-1663.
26. Magyari, K., V. Simon, and G. Varo 2006. The influence of the halide ions on the photochemical reaction cycle of pharaonis halorhodopsin. J Photochem Photobiol B, *82:* 16-20.
27. Schobert, B. and J. K. Lanyi 1986. Electrostatic interaction between anions bound to site I and the retinal Schiff base of halorhodopsin. Biochemistry, *25:* 4163-4167.
28. Shibata, M., N. Muneda, T. Sasaki, K. Shimono, N. Kamo, M. Demura, and H. Kandori 2005. Hydrogen-Bonding Alterations of the Protonated Schiff Base and Water Molecule in the Chloride Pump of Natronobacterium pharaonis. Biochemistry, *44:* 12279-12286.
29. Michel, H. and D. Oesterhelt 1976. Light-induced changes of the pH gradient and the membrane potential in H. halobium. FEBS Lett, *65:* 175-178.
30. Nagel, G., B. Kelety, B. Mockel, G. Buldt, and E. Bamberg 1998. Voltage dependence of proton pumping by bacteriorhodopsin is regulated by the voltage-sensitive ratio of M1 to M2. Biophys J, *74:* 403-412.
31. Luecke, H., B. Schobert, H. T. Richter, J. P. Cartailler, and J. K. Lanyi 1999. Structural changes in bacteriorhodopsin during ion transport at 2 angstrom resolution. Science, *286:* 255-261.
32. Lanyi, J. K. and H. Luecke 2001. Bacteriorhodopsin. Curr Opin Struct Biol, *11:* 415-419.
33. Robinson, R. A. and R. H. Stokes 1959. Electrolyte solution, 2nd ed. edition. London: Butterworth.
34. Israelachvili, J. 1992. Intermolecular and Surface Forces. New York: Academic Press Ltd.

Table I Kinetic parameters for anion transport via *p*HR in the voltage-clamped oocytes at -50 mV. The photo-induced currents indicating anion transport rates at -50 mV were determined with increasing concentrations of the anion substrates (1 - 100 mM). The experiment was repeated with five oocytes. The values for $K_{0.5}$ and I_{max} were calculated with a Michaelis-Menten type equation (Eq.1). Data represent the mean ± SE (n = 5).

Ion	Kinetic parameters	
	$K_{0.5}$ (mM)	I_{max} (nA)
Cl^-	24.0 ± 2.5	324 ± 22
Br^-	11.2 ± 1.3	280 ±27
I^-	17.2 ± 1.3	243 ± 20
NO_3^-	45.5 ± 3.8	193 ± 21
SCN^-	27.4 ± 2.0	160 ± 19

Figure Legends

Figure 1 Traces of representative photo-induced currents via *p*HR expressed heterologously in *Xenopus* oocytes

*p*HR-expressing oocytes were superfused with standard buffer containing different anions (as sodium salts) at a concentration of 100 mM. The hatched bars below the current traces indicate the period (10 sec) of illumination with green light (530±18 nm). In control oocytes with no *p*HR expression, there were no detectable currents in responses to light pulses (data not shown).

Figure 2 Substrate specificity of *p*HR

(A) Representative current-voltage relationship (*I-V* curve) at steady state for *p*HR-mediated photo-induced currents in the presence of different anions (as sodium salts) (100 mM)**. (B)** Outward photo-induced currents at -50 mV in the presence of various anions. The concentration of anions (as sodium salts) in the perfusion medium was 100 mM. **(C)** Reversal potentials for the anion pump activity of *p*HR with different anions. The current-voltage (*I-V*) relationship was linear for all anions tested. Reversal potentials were estimated from the x-intercepts (*i.e.*, zero current) with the extrapolation of the lines describing the *I-V* relationship. Data represent mean ± SE (n = 4- 6).

Figure 3 Relationship of the Cl^- pump activity of *p*HR to the light intensity (A) and membrane potential (B)

The photo-induced currents in the presence of 100 mM Cl^- were determined at steady state in *p*HR-expressing oocytes at different light intensities. The light intensity was measured with a photometer and expressed as % of maximal light intensity. **(A)** The dependence of photo-induced current at -50 mV on light intensity. **(B)** The dependence of photo-induced current on membrane potential at different light intensities. The reversal potential was estimated from the x-intercepts by the extrapolation of the lines describing the *I-V* relationship. The reversal potentials remained unchanged irrespective of the light-intensity. The inset in **(B)** represents the dependency of reversal potential on the light intensity. Data represent mean ± SE (n = 7-10).

Figure 4 Reversal potentials for wild-type and mutant (R123K) *p*HRs

(A) Representative current-voltage relationship (*I-V* curve) at steady state for wild-type and mutant (R123K) *p*HRs. The concentration of Cl^- in the perfusion medium (as NaCl) was 100 mM. **(B)** Reversal potentials for wild-type and mutant (R123K) *p*HRs. The values were determined from the x-intercepts by the extrapolation of the lines describing the *I-V* relationship. Data represent mean ± SE (n = 6).

Figure 5 Saturation kinetics of the photo-induced Cl^- pump activity of *p*HR

(A) Representative current-voltage relationship (*I-V* curve) at steady state in *p*HR-expressing oocytes at increasing concentrations of Cl^- (as NaCl) (1 – 100 mM). **(B)** Photo-induced currents at -50 mV indicative of Cl^- entry as a function of Cl^- concentration. The experiment was repeated five times with different oocytes. Since the expression levels of *p*HR varied among the oocytes, data were normalized by the value of I_{max} calculated with Eq.1 in each oocyte. The inset shows the Eadie-Hofstee plot. The $K_{0.5}$ and I_{max} values calculated with a Michaelis-Menten type equation (Eq.1) were 24.0 ± 2.5 (±SE) mM and 324 ± 22 (±SE) nA, respectively. Data represent mean ± SE (n = 5).

Figure 6 Influence of membrane potential on $K_{0.5}$ (*i.e.* concentration of Cl^- needed for the half-maximal photo-induced current) (A) and I_{max} (*i.e.* the maximal photo-induced current at saturating concentrations of Cl^-) (B) in *p*HR-expressing oocytes.

Figure 7 Results of the global fitting of the flash-photolysis data of wild-type *p*HR

(A) Absorption spectra of unphotolyzed (ground) state (P_0, ▬) and four kinetically distinguishable intermediates at three representative Cl^- concentrations (———, 50mM; --- , 400 mM; · · ·, 1000 mM) . P_3 state shows the largest dependence on Cl^- concentration, both in terms of the time constant (τ_3) and the absorption spectrum. The figures represent the time constants corresponding to the states in 50 mM NaCl, pH7.0 at 20 ^oC. **(B)** Time constants for the photochemical transitions as a function of Cl^- concentrtation.

Figure 8 Dependence of $K_{0.5}$ on the limiting equivalent conductivities (λ^0) of anions in water (A) and that of I_{max} on the dehydrated radii (B)

The values for the limiting equivalent conductivities (λ^0) of anions in water and the dehydrated radii were taken from published reports (33, 34).

Figure 9 A kinetic model for the photo-induced current at steady state for *p*HR on the basis of the photocycle

Under conditions of continuous illumination, all intermediates attain steady state and the excited *p*HR consists almost entirely of the population of the intermediate molecules in the rate determining transition and the photo-induced current is governed mainly by the rate determining process. Therefore, focusing only on the intermediates involved in the photo-induced current at steady state, we simplify the photocycle scheme of *p*HR and construct the kinetic model describing the photo-induced current due to Cl^- transport via *p*HR. The kinetic model is comprised of two processes: one is the fast transition of intermediates corresponding to Cl^- translocating and releasing processes, and the other is the rate determining transition corresponding to Cl^- binding processes. According to the mass conservation, a mass-balance equation consists of the original *p*HR, the photo-excited *p*HR (*p*HR*) molecules, and Cl^- free and bound intermediates (X_{free} and X_{bound}, respectively). Taking into consideration that the k_{rate} value is much smaller than any other rate constants (k_{fast}, k_a and k_d), the photo-induced current at steady state is reduced to Eq.3.

Fig.1

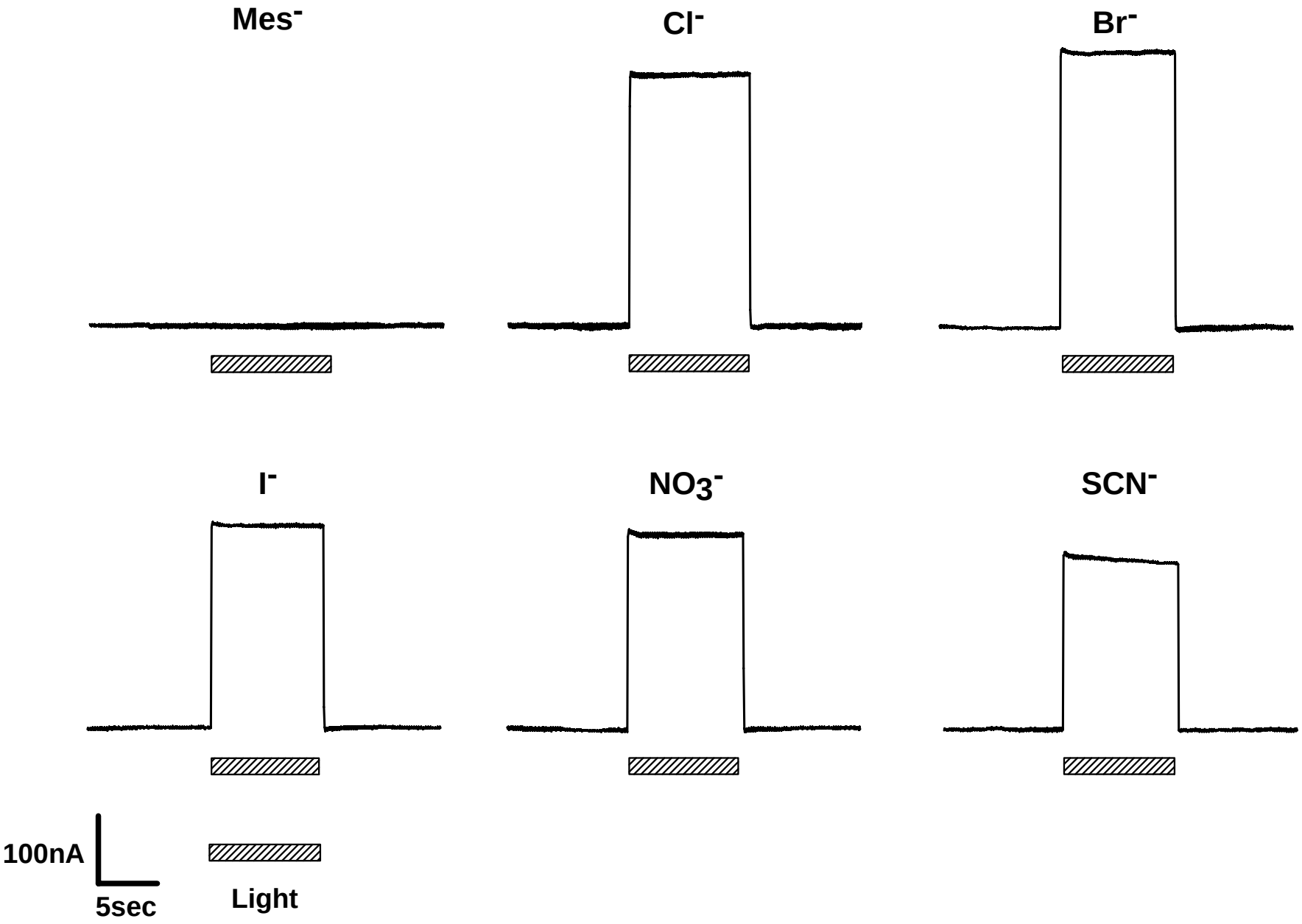

Fig.2

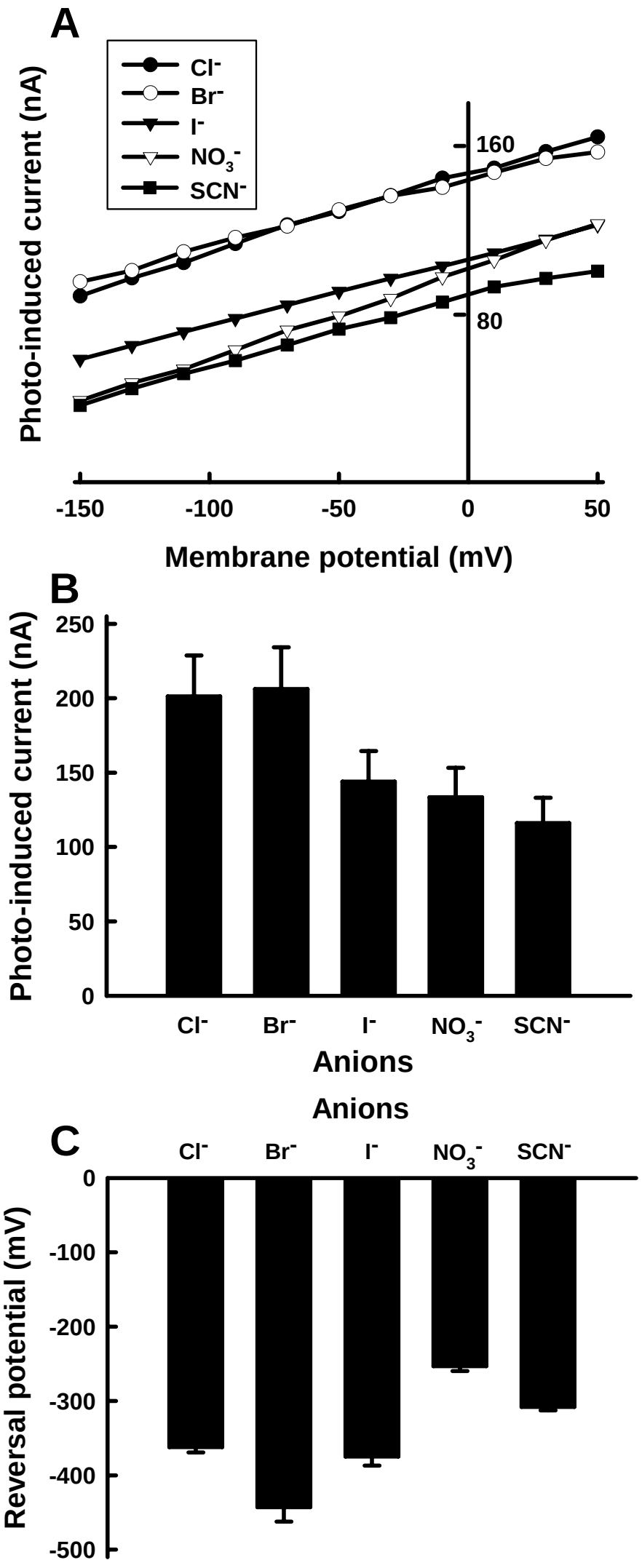
A
Cl-
Br-
I-
NO3-
SCN-
160
80
Photo-induced current (nA)
-150
-100
-50
0
50
Membrane potential (mV)
B
250
200
150
100
50
0
Photo-induced current (nA)
Cl-
Br-
I-
NO3-
SCN-
Anions
Anions
C
Cl-
Br-
I-
NO3-
SCN-
0
-100
-200
-300
-400
-500
Reversal potential (mV)

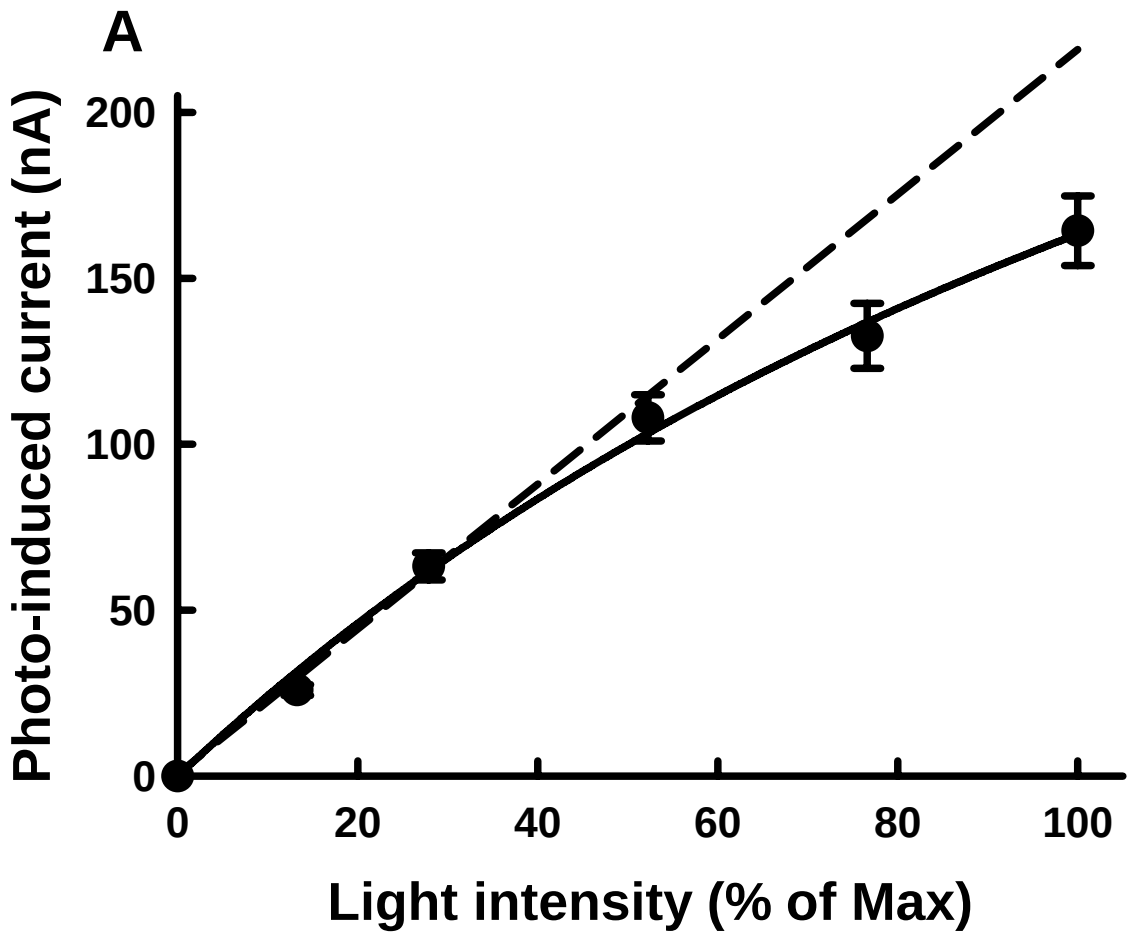
A
Photo-induced current (nA)
200
150
100
50
0
0
20
40
60
80
100
Light intensity (% of Max)

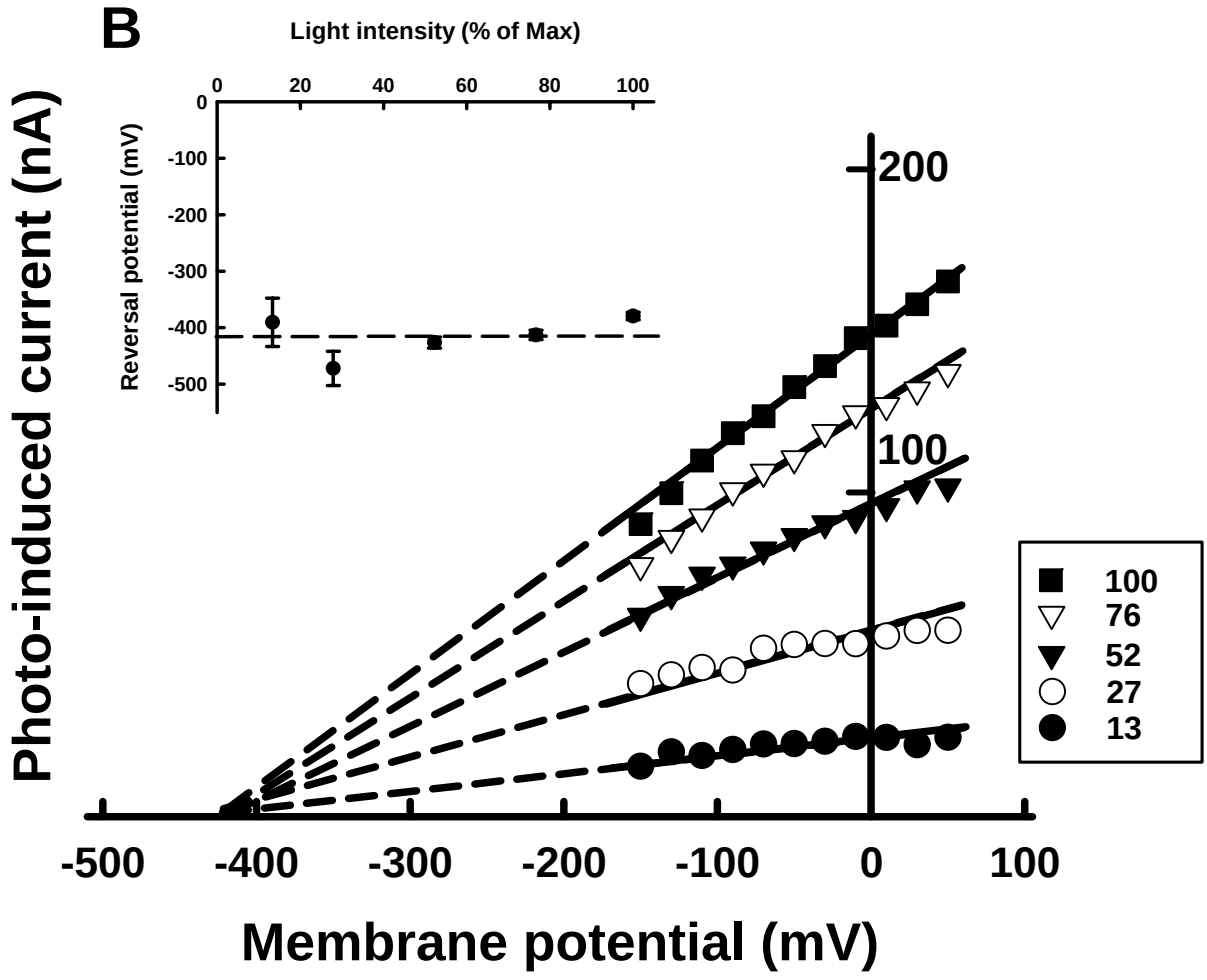
B
Light intensity (% of Max)
0
20
40
60
80
100
Reversal potential (mV)
0
-100
-200
-300
-400
-500
Photo-induced current (nA)
200
100
100
76
52
27
13
-500
-400
-300
-200
-100
0
100
Membrane potential (mV)

Fig.4

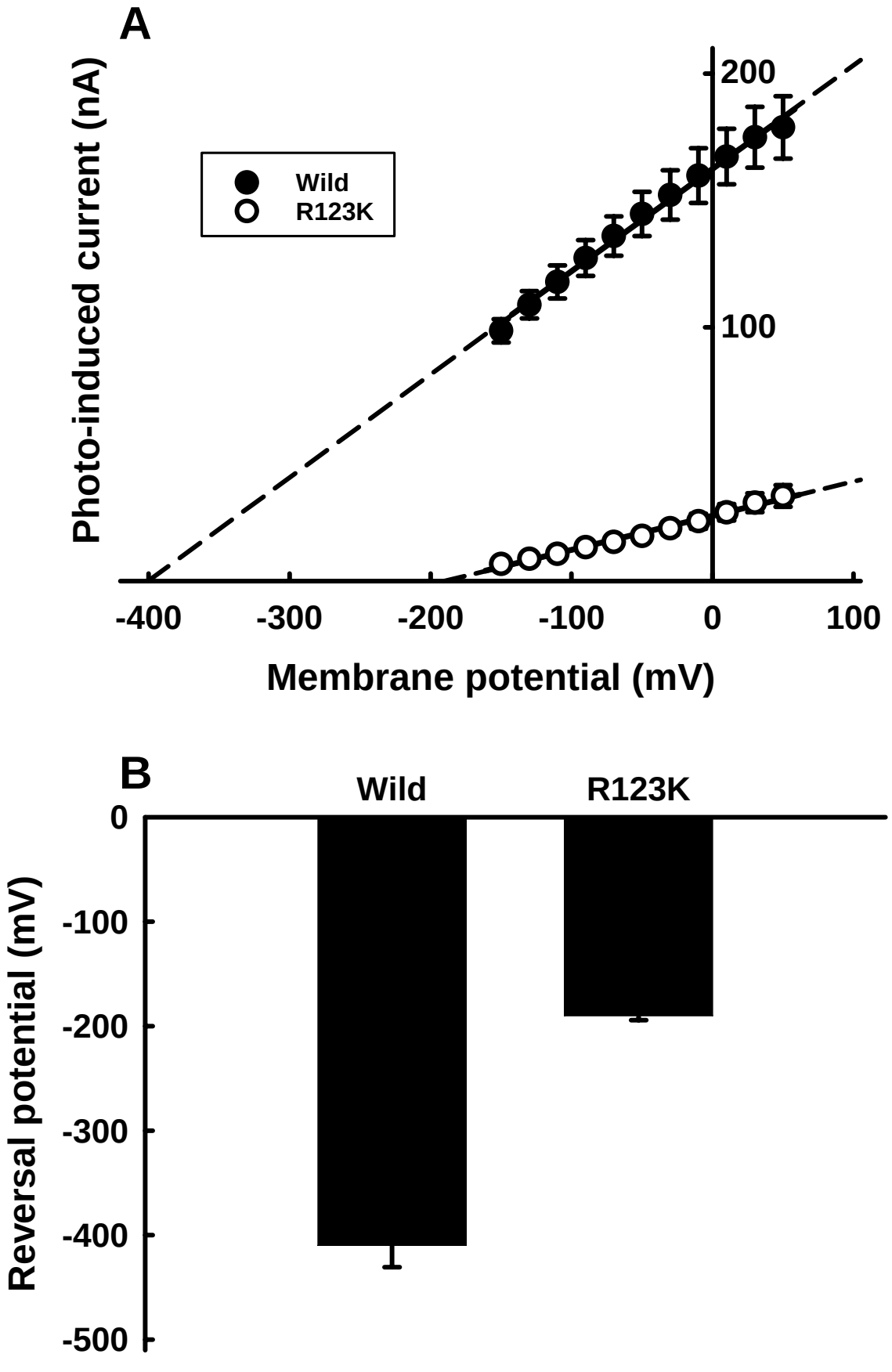
A
Photo-induced current (nA)
200
100
Wild
R123K
-400
-300
-200
-100
0
100
Membrane potential (mV)
B
Wild
R123K
0
-100
-200
-300
-400
-500
Reversal potential (mV)

Fig.5

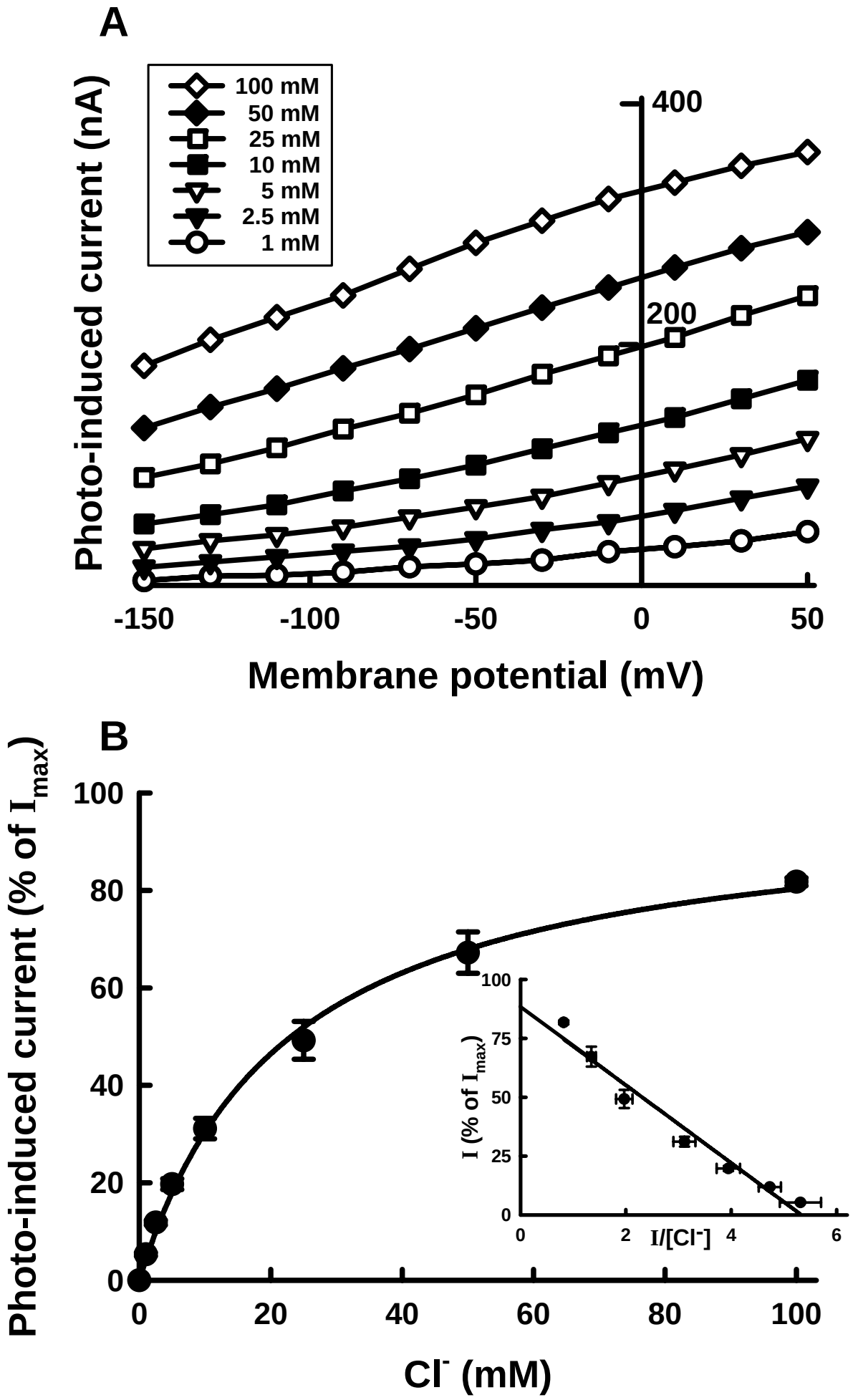
A
100 mM
50 mM
25 mM
10 mM
5 mM
2.5 mM
1 mM
Photo-induced current (nA)
400
200
-150
-100
-50
0
50
Membrane potential (mV)
B
Photo-induced current (% of I_max)
100
80
60
40
20
0
0
20
40
60
80
100
Cl- (mM)
I (% of I_max)
100
75
50
25
0
0
2
I/[Cl-]
4
6

Fig.6

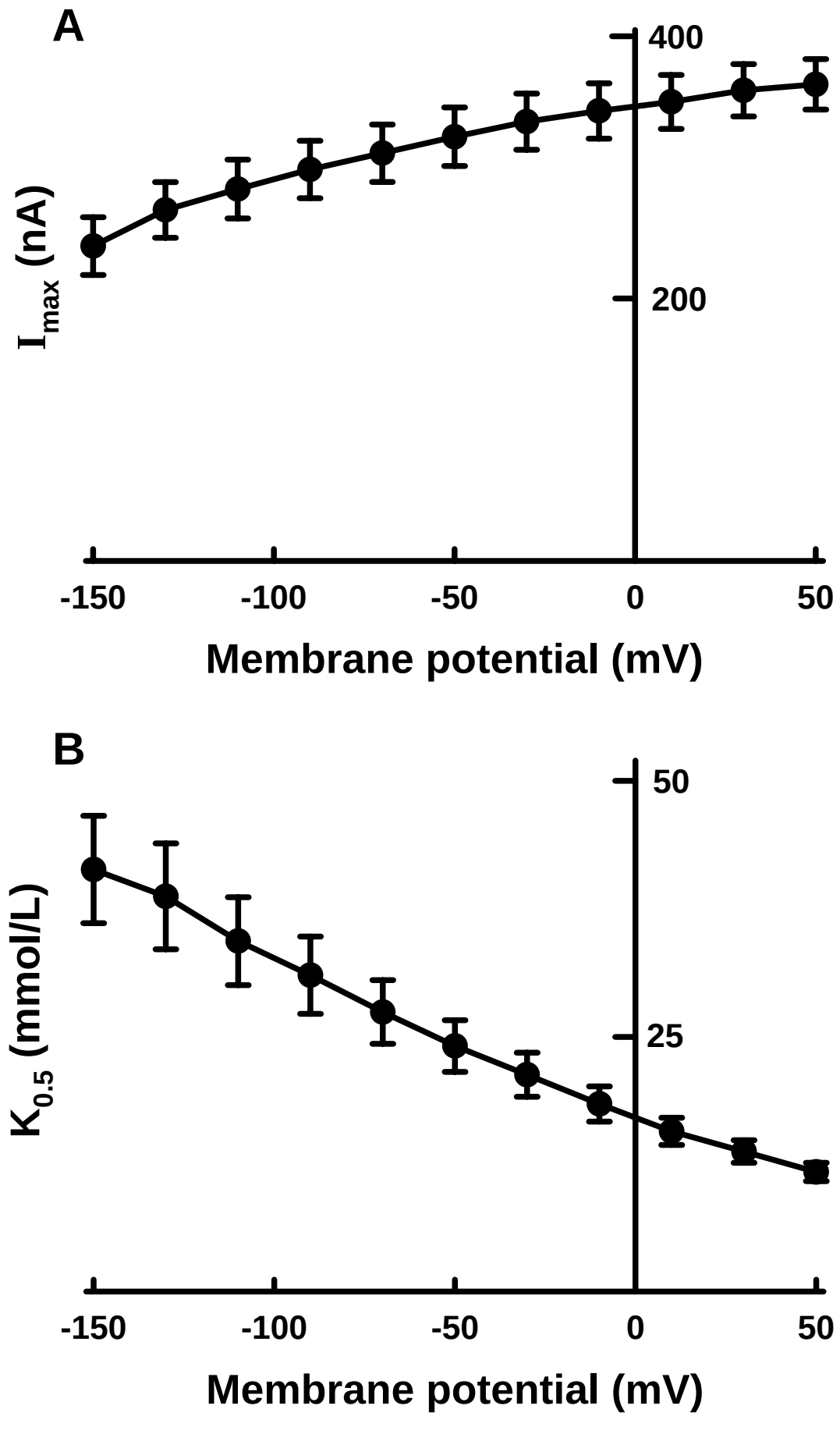
A
400
200
I_{max} (nA)
-150
-100
-50
0
50
Membrane potential (mV)
B
50
25
$K_{0.5}$ (mmol/L)
-150
-100
-50
0
50
Membrane potential (mV)

Fig. 7

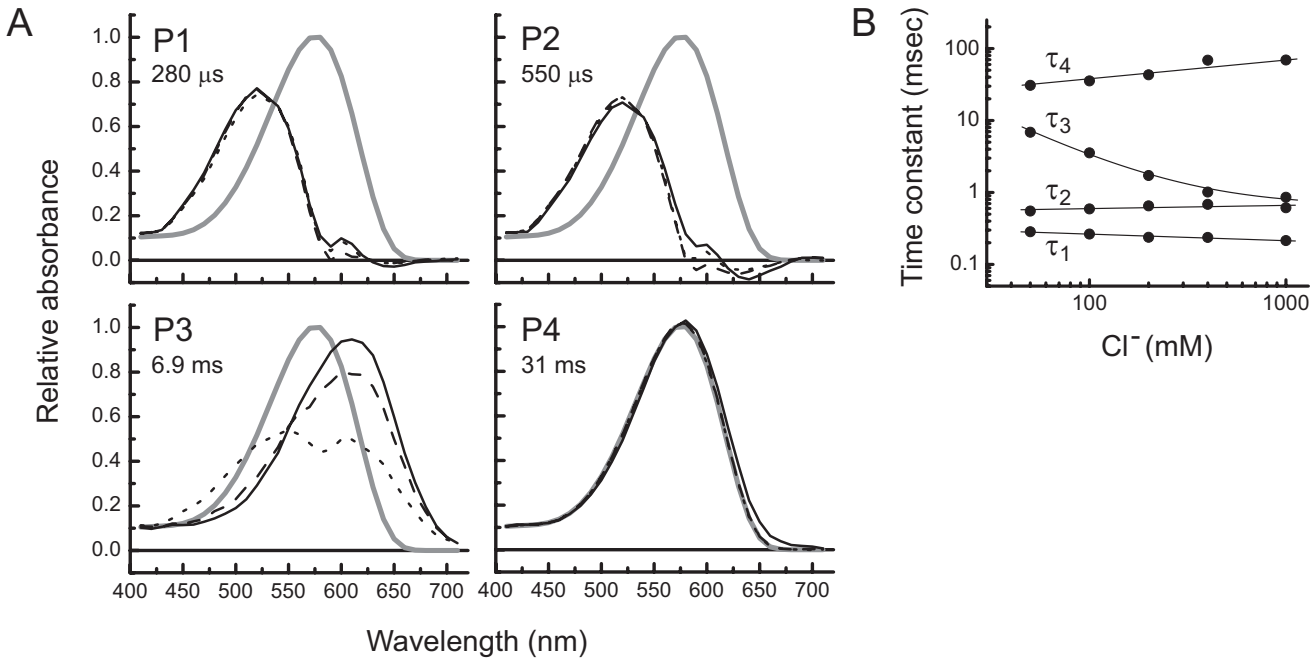
A
P1
280 μs
P2
550 μs
P3
6.9 ms
P4
31 ms
Relative absorbance
1.0
0.8
0.6
0.4
0.2
0.0
400 450 500 550 600 650 700
Wavelength (nm)
B
Time constant (msec)
100
10
1
0.1
τ4
τ3
τ2
τ1
100
1000
Cl⁻ (mM)

Fig.8

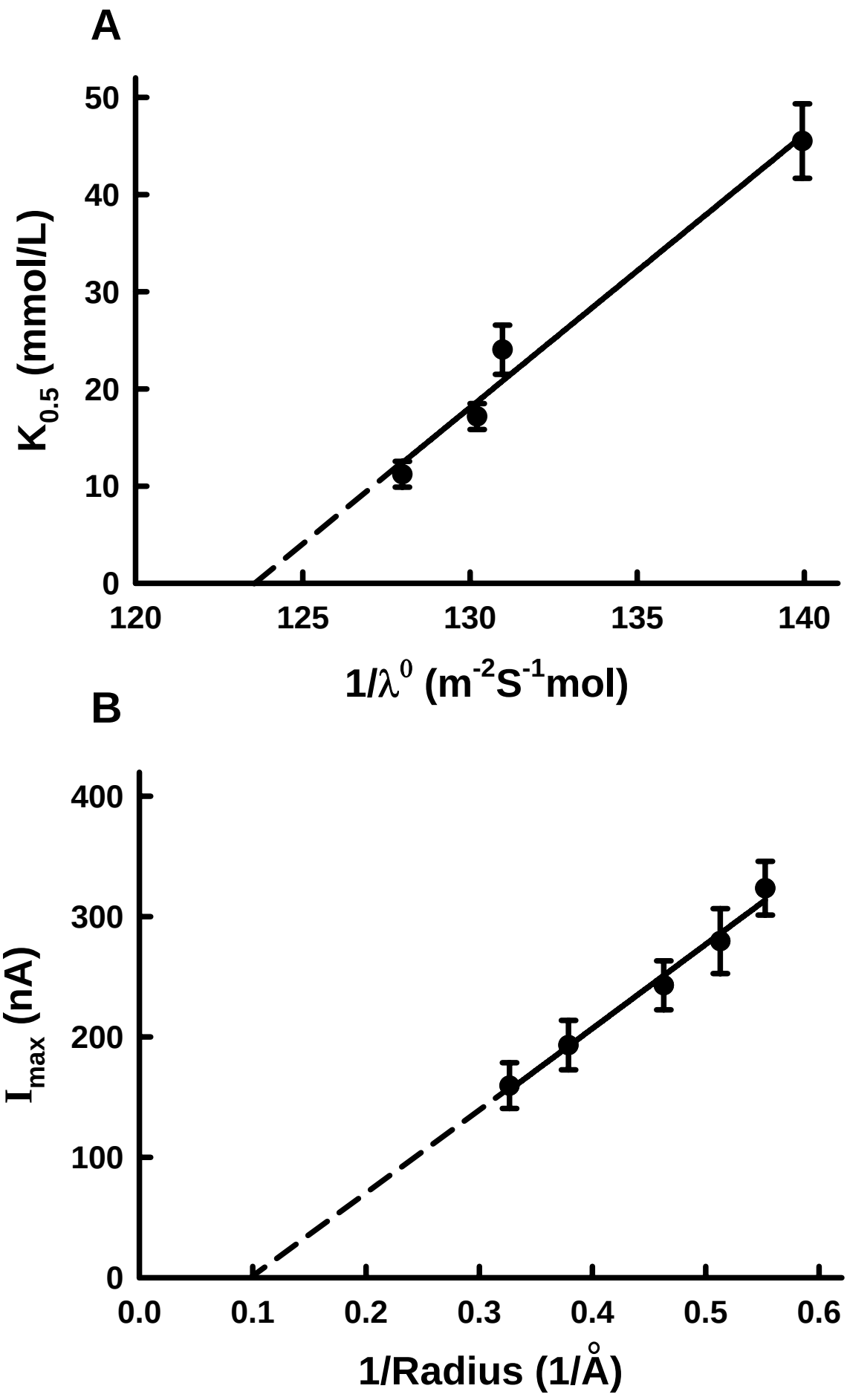
A
50
40
30
20
10
0
120
125
130
135
140
$K_{0.5}$ (mmol/L)
$1/\lambda^0$ ($m^{-2}S^{-1}mol$)
B
400
300
200
100
0
0.0
0.1
0.2
0.3
0.4
0.5
0.6
I_{max} (nA)
1/Radius (1/Å)

Fig.9

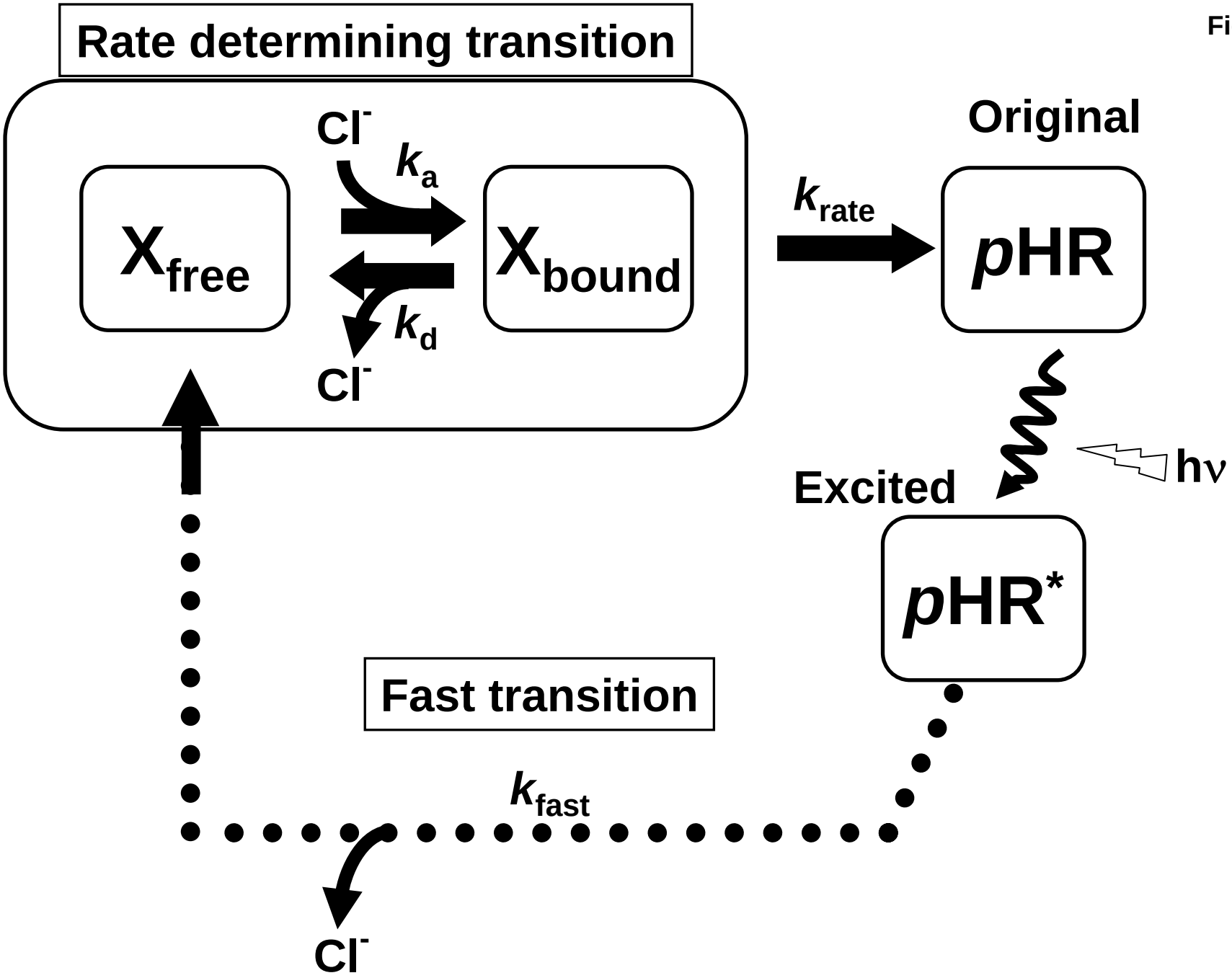
Rate determining transition
Cl-
ka
Xfree
Xbound
kd
Cl-
Original
krate
pHR
Excited
hν
pHR*
Fast transition
kfast
Cl-